

# TECTONOMETAMORPHIC EVOLUTION OF BLUESCHIST-FACIES ROCKS IN THE PHYLLITE-QUARTZITE UNIT OF THE EXTERNAL HELLENIDES (MANI, GREECE)

Peter MICHEUZ, Kurt KRENN<sup>1</sup>, Harald FRITZ & Walter KURZ

DOI: 10.17738/ajes.2015.0007

## KEYWORDS

fluid inclusions  
constriction  
blueschists  
Greece  
Mani

Institute of Earth Sciences, Member of NAWI Graz, University of Graz, Universitätsplatz 2, A-8010 Graz, Austria;

<sup>1</sup> Corresponding author, kurt.krenn@uni-graz.at

## ABSTRACT

The Phyllite-Quartzite Unit of the southern Peloponnese (Mani, Greece) experienced HP-LT metamorphism as result of northeastward-directed subduction of the Adriatic plate beneath the Eurasian plate during the Late Oligocene to Early Miocene. On the basis of macro- and microstructures and quartz textures the Phyllite-Quartzite Unit experienced four deformation stages that have been linked with an already proposed age range from literature: D1-uniaxial stretching at about 29-24 Ma, D2-rotational shearing and folding at ca. 24-19 Ma, D3-folding at ca. 19 Ma and D4-extension at 19-15 Ma. D2-related shear folds F2 and subsequent open folds F3 (D3) form a large-scale fold interference pattern including relics of F1-constriction folds. Blueschist-facies micaschists contain chloritoid 1 porphyroblasts including an earliest foliation S1 which was overprinted by SSW directed shearing (D2). Blueschists show syngenetic chloritoid 1 and glaucophane, both rotated parallel to the dominant foliation S2 defined by mica and graphite. Fluid inclusion microthermometry was performed on concordant quartz layers (Qtz1) as well as discordant D4-related extensional quartz veins (Qtz2). Fluid data combined with rheological characteristics have been used to constrain conditions for deformation stages along a published P-T path representative for the southern Peloponnese. Fluid density isochores related to Qtz1 indicate density loss from peak conditions down to ca. 6 kbars along non-isochoric exhumation (isothermal decompression between 450-500°C) and deformation stages D1-D3. Conditions < 6 kbar and 400°C for deformation stage D4 have been derived from primary fluid inclusions in Qtz2 subsequent to isobaric cooling.

Die Phyllit-Quarzit Einheit der südlichen Peloponnes Halbinsel (Mani, Griechenland) zeigt Hochdruck-Niedrigtemperaturmetamorphose als Resultat einer Nordost gerichteten Subduktion der Adriatischen Platte unter die Eurasische Platte im Späten Oligozän bis Frühen Miozän. Anhand von Mikrostrukturen und Quarztexturen können für die Phyllit-Quarzit Einheit vier Deformationsereignisse mit bereits publizierten Altersdaten in Verbindung gebracht werden: D1 – uniaxiale Streckung um ca. 29-24 Ma, D2 – Scherung und Faltung um 24-19 Ma, D3 – offene Faltung um ca. 19 Ma und D4 – Dehnung um 19-15 Ma. Die Überlagerung von D2-Scherfalten mit D3-bezogenen offenen Falten resultiert in großräumig kartierten Falteninterferenzmustern welche D1-bezogene uniaxiale Falten beinhalten. Blauschieferfazielle Glimmerschiefer zeigen rotierte Chloritoid- Porphyroblasten mit einem Interngefüge S1 überprägt von D2-bezogener SSW-gerichteter Scherung. Blauschiefer beinhalten syngenetischen Chloritoid und Glaukophan, welche in einer Matrix bestehend aus Hellglimmer und Graphit während D2 einrotiert wurden. Flüssigkeitseinschlussmikrothermometrie konnte an konkordantem Quarz (Qtz1) sowie diskordantem D4- Quarzgängen (Qtz2) durchgeführt werden. Mittels rheologischen Kriterien und Daten aus Flüssigkeitseinschlüssen (Dichte und Zusammensetzung) wurden die Bedingungen der einzelnen Deformationsphasen mit Hilfe eines bereits publizierten P-T Pfades repräsentativ für die südliche Peloponnes Halbinsel abgeleitet. Aus Dichteisochoren für Qtz1 lässt sich ein Druckverlust von Maximalbedingungen bis ca. 6 kbar entlang isothermaler Dekompression (450-500°C), einhergehend mit Deformationsstadien D1-D3, ermitteln. Bedingungen unter 6 kbar und 400°C für D4 können aus primären Flüssigkeitseinschlüssen in Qtz2, gefolgt von isobarem Abkühlen vorgeschlagen werden.

## 1. INTRODUCTION

High pressure-low temperature (HP-LT) rocks are used to determine mineral reactions in subduction zones during subduction and exhumation. Related ductile structures can record early deformation stages during and after peak metamorphism. Minimum conditions for ductile and brittle deformation overprint can be determined by fluid inclusion microthermometry on early concordant and late discordant quartz-bearing veins (e.g. Lespinasse and Pechêr, 1986; Boullier et al., 1991; 1999; Krenn et al., 2008; Krenn, 2010). In the External Hellenides, the Phyllite-Quartzite Unit contains blueschist-facies rocks of Oligocene-Miocene age that record a HP-LT evolution (e.g. Katagas,

1980; Seidel et al., 1982, Doutsos et al., 2000; Ring et al., 2001). Previous studies related to the Phyllite-Quartzite Unit focused on regions on Crete and the central Peloponnese but are rare on the Mani peninsula in the southern Peloponnese (e.g. Chatzaras et. al., 2006; Jolivet et al., 2010). Here, fluid inclusion microthermometry linked with structural data is presented in order to constrain the tectonometamorphic history of the Phyllite-Quartzite Unit.

## 2. GEOLOGICAL SETTING

The Hellenides as part of the Alpine orogen extend from

northwestern Greece to the Peloponnese and continue towards Crete and Rhodos (Fig. 1). They are divided into an internal and external part by the Pindos Ophiolitic Suture Zone (Smith et al., 1979; Robertson, 2002; Stampfli and Borel, 2004) or defined to the Pindos Zone without evidence of a former oceanic suture (Schmid et al. 2008 and references therein). The external part contains a HP-LT belt which contours the Hellenic arc. HP-LT metamorphism resulted from northeastward subduction of Adriatic-derived thrust sheets (southern realm of the Adriatic indenter after Schmid et al., 2008) beneath the Eurasian plate which was followed by up to 1000 km of south-directed slab retreat during Late Oligocene – Miocene time (e.g. Jolivet and Faccenna, 2000; Jolivet et al., 2003). Most recent works propose that the high pressure units of the External Hellenides were exhumed during sustained underplating which compensated crustal thinning along a N (E)- dipping detachment in the hanging-wall of the Phyllite-Quartzite Unit (Ring et al., 2001; 2007; Ring and Reischmann, 2002; Kiliias et al., 1994; Jolivet et al., 1994; Xypolias and Koukouvelas, 2001).

Tectonostratigraphically, the External Hellenides are divided into upper and lower tectonic units (Fig. 2). The lower tectonic units consist of the Plattenkalk unit at the base and the

Phyllite-Quartzite Unit at the top. The peak metamorphism of and Reischmann, 2002; Kiliias et al., 1994; Jolivet et al., these units occurred during Late Oligocene to Early Miocene times (e.g. Kiliias et al., 1994; Fassoulas et al., 1994; Chatzaras et al., 2006). In contrast, the upper tectonic units have not suffe-

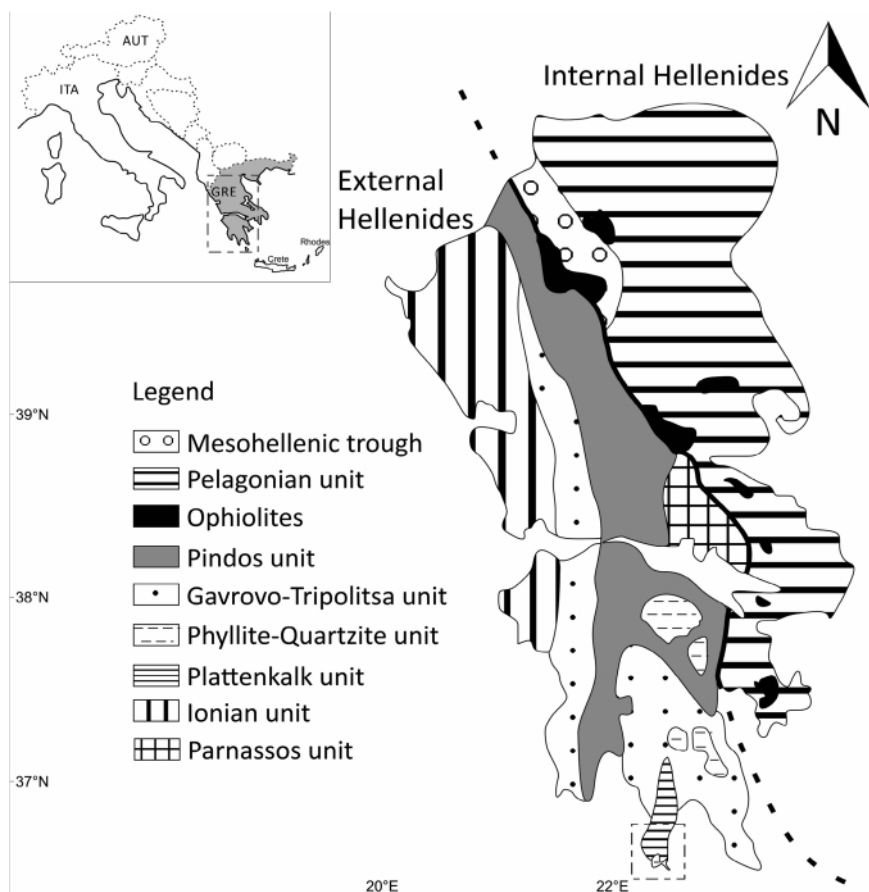


**FIGURE 1:** Geological overview of the Hellenides after Jacobshagen (1986) and modified by Doutsos et al. (2006). The rectangle displays the southernmost area of the Peloponnese and indicates the study area on the Mani peninsula.

Main tectonic units		Lithology / protolith age	Peak metamorphic conditions age
Upper tectonic units	Uppermost unit	<ul style="list-style-type: none"> <li> Serpentinites (<i>Ophiolitic subunit</i>) / Upper Jurassic</li> <li> Amphibolites, gneisses, pillow-lavas, pelagic limestones and clastic sediments (<i>Ophiolitic mélange</i>) / Upper Jurassic</li> </ul>	low-pressure/high-temperature (4-6 kbar/650-700°C) Late Cretaceous
	Pindos unit	<ul style="list-style-type: none"> <li> Flysch deposits / Eocene</li> <li> Deep-water carbonate rocks / Triassic-Paleocene</li> </ul>	—
	Tripolitsa unit	<ul style="list-style-type: none"> <li> Flysch deposits / Upper Eocene-Oligocene</li> <li> Shallow-water carbonate rocks / Triassic-Eocene</li> </ul>	low-pressure/low-temperature (~ 3 kbar/~ 250°C)
Lower tectonic units	Phyllite-Quartzite unit	<ul style="list-style-type: none"> <li> Foliated massive marbles and metavolcanic rocks (<i>Vasiliko unit</i>)</li> <li> Phyllites, quartzites and metaconglomerates with marble intercalations / Upper Carboniferous-Triassic</li> </ul>	unknown high-pressure/low-temperature (10 ± 3 kbar/400 ± 50°C) Late Oligocene-Early Miocene
	Plattenkalk unit	<ul style="list-style-type: none"> <li> Flysch deposits / Middle Oligocene</li> <li> Marbles with nodular cherts / Lower Jurassic-Eocene</li> <li> Dolomitic marbles / Upper Triassic-L. Jurassic</li> <li> Marbles and schists / Upper Carboniferous-Upper Triassic</li> </ul>	high-pressure/low-temperature (7 - 10 kbar/~ 350°C) Late Oligocene-Early Miocene

**FIGURE 2:** Main tectonic units of the External Hellenides after Chatzaras et al. (2006). Circle shows tectonostratigraphic level of the study area.

red the Oligocene-Miocene high-pressure metamorphism and are characterized as cover thrust sheets.

The allochthonous Phyllite-Quartzite Unit is represented by phyllites, quartzites, metaconglomerates and marbles and corresponds to an Upper Carboniferous to Triassic rift sequence (Robertson, 2006). Trotet et al. (2006) differentiated the Phyllite-Quartzite Unit by its metamorphic evolution into the Alagonia Unit composed of greenschist-facies micaschists with chloritoid and albite; the Metaconglomerate Unit consisting of

blueschist-facies metaconglomerates and micaschists; the Lada Unit built up by high-temperature (HT) blueschist-facies micaschists with garnet and glaucophane and the Blueschist Unit made up of blueschist-facies micaschists with chloritoid and lenses of glaucophanite. The underlying Plattenkalk Unit is represented by layers of Upper Carboniferous to Eocene carbonates (Bonneau, 1973; Krahl et al., 1988) with a thin succession of Middle Oligocene flysch on top (Bizon et al., 1976) (Fig. 2). On the Peloponnese the lack of HP-LT mine-

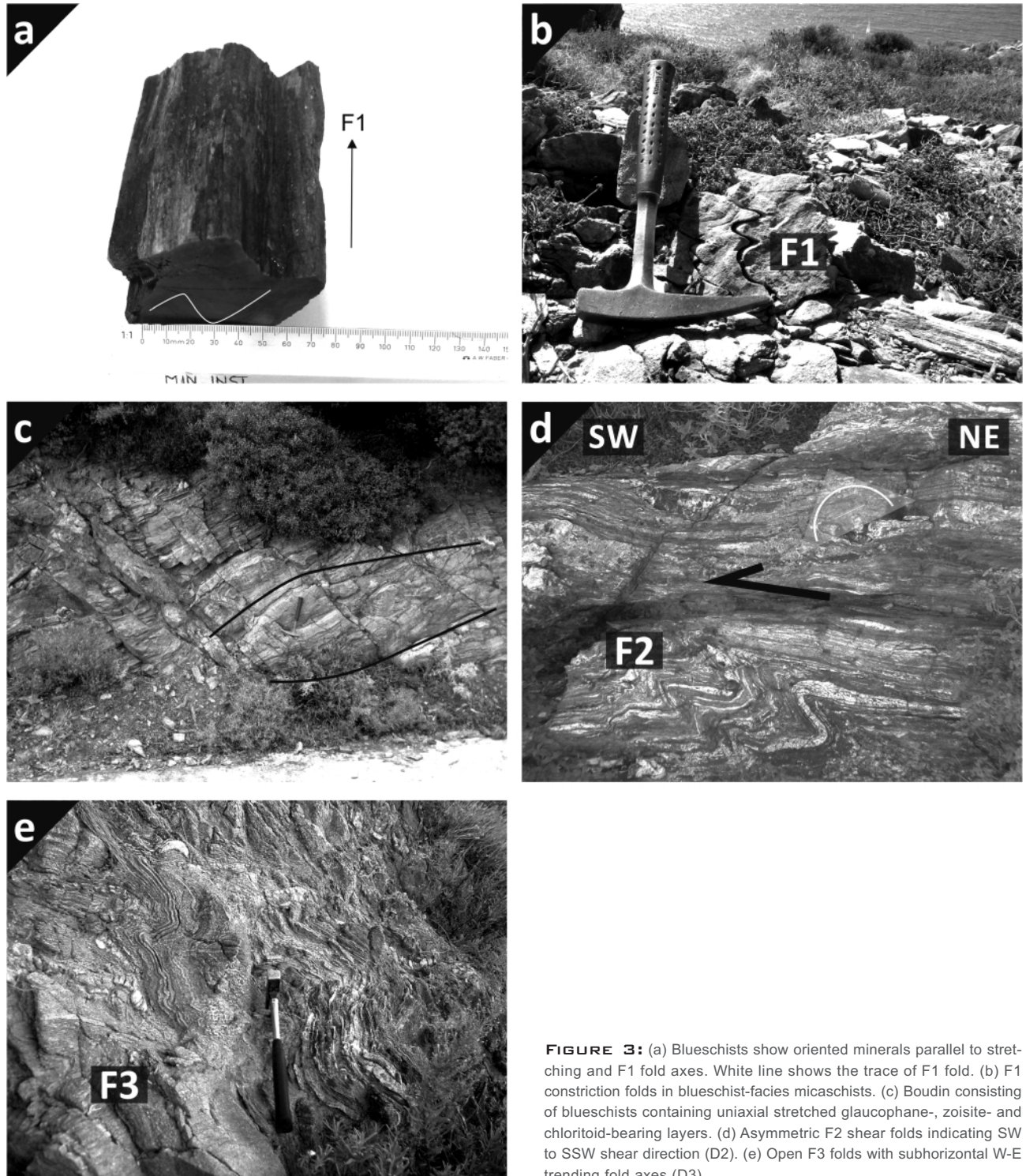


**FIGURE 3:** (a) Blueschists show oriented minerals parallel to stretching and F1 fold axes. White line shows the trace of F1 fold. (b) F1 constriction folds in blueschist-facies micaschists. (c) Boudin consisting of blueschists containing uniaxial stretched glaucophane-, zoisite- and chloritoid-bearing layers. (d) Asymmetric F2 shear folds indicating SW to SSW shear direction (D2). (e) Open F3 folds with subhorizontal W-E trending fold axes (D3).

erals within the Plattenkalk Unit supports the assumption that the Phyllite-Quartzite Unit was thrust onto the Plattenkalk Unit during exhumation from high-pressure conditions (e.g. Doutsos et al., 2000). According to Blumör et al. (1994) P-T conditions for the Plattenkalk Unit on the Peloponnese are 7 - 8 kbar and 310 - 360°C.

The timing of deformation stages in this area may be simultaneously to deformation described in western Crete after Chatzaras et al. (2013) and references therein. Early SSE-directed nappe stacking linked with N-ward subduction of the Plattenkalk Unit and Phyllite-Quartzite Unit occurred around 36-29 Ma and culminated between 24-19 Ma. Subsequent ductile exhumation of the Phyllite Quartzite Unit from ca. 35 up to ca. 10 km occurred at 17-15 Ma whereas latest cooling ages < 100°C lie around 14 Ma accompanied with latest SW-directed out-of-sequence brittle-thrust faulting and fault propagation folding.

Peak metamorphism within the Phyllite-Quartzite Unit changes from the northern Peloponnese to Crete due to (a) different velocities of slab retreat, (b) the type of subduction channel and (c) the circulation characteristics of exhuming material (Jolivet et al., 2010). Thus temperature variations from 550°C

in the northern part of the Peloponnese down to 400 ± 50°C in Crete at peak pressures of ~ 13 - 18 kbar occur. In the investigated area peak conditions for the Phyllite-Quartzite Unit are 13 - 17 kbar and ca. 450°C (e.g. Xypolias et al., 2007).

### 3. ANALYTICAL METHODS

Mineral chemical analysis of silicate phases on polished thin sections was performed with a scanning electron microscope JEOL JSM-6310, attached to a wavelength dispersive system with an acceleration voltage of 15 kV, at the University of Graz, Institute of Earth Sciences (Department of Mineralogy and Petrology).

Lattice preferred orientation (LPO) patterns of quartz were measured to analyse deformation geometries and shear senses. For this, the software package "crystal imaging system G50 Fabric Analyser" by Russell-Head Instruments was used to estimate quartz <c> axis [001] orientations. Shear senses have been determined with respect to the stretching lineation.

To obtain minimum conditions for deformation stages in the Phyllite-Quartzite Unit fluid inclusion microthermometry was performed on quartz veins which occur parallel (concordant)

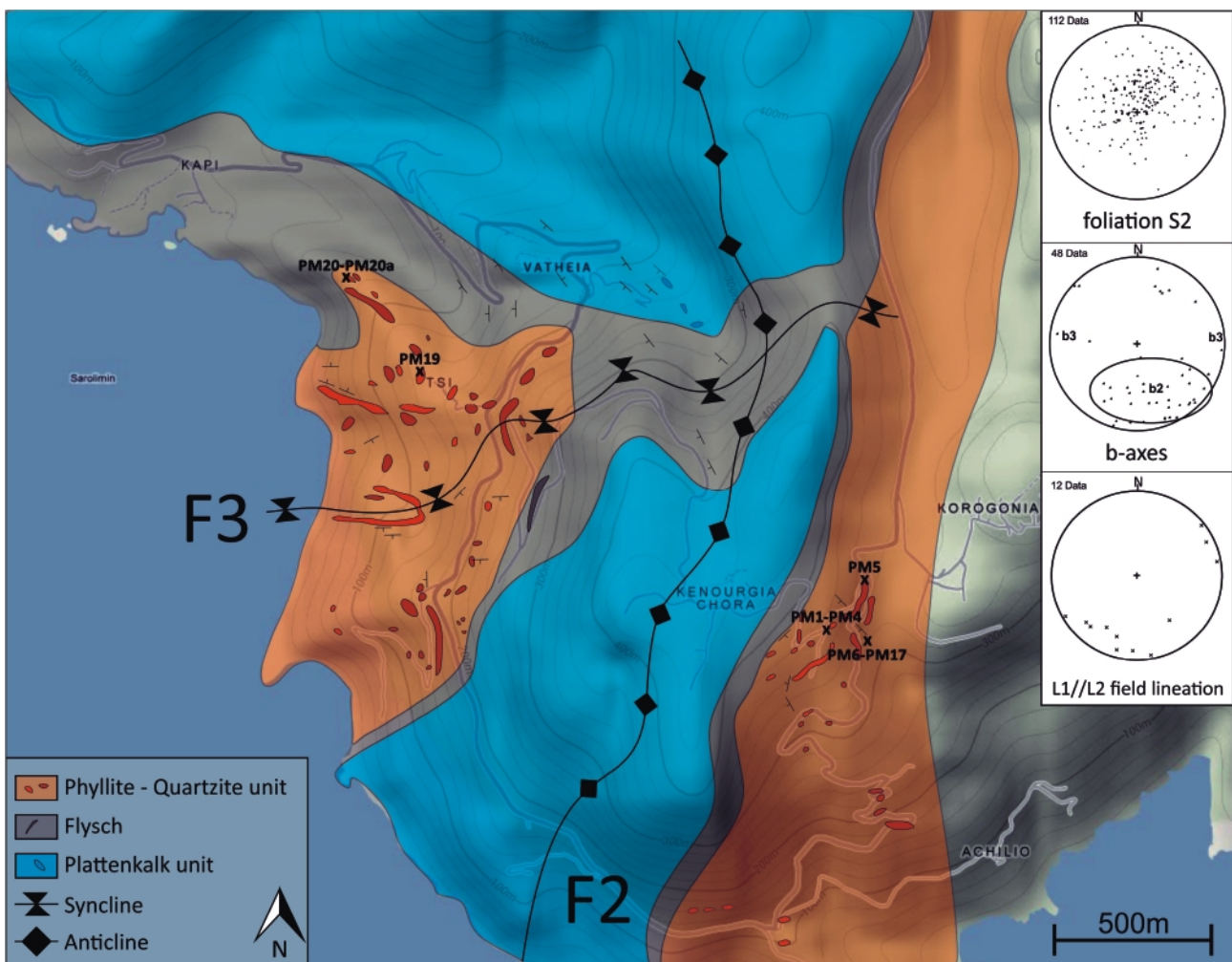


**FIGURE 4:** Mapped area of the Mani peninsula. A large-scale fold interference pattern results from superposition of F2 and F3. Tectonic contacts are not characterized and the trace of the fold structure is not exactly supported by field outcrops. Field data result from areas which are indicated by more intense colours and geologic symbols.

and perpendicular (discordant) to the foliation. Primary fluid inclusions should additionally give important information about the fluid which was present during quartz vein precipitation. Fluid inclusion microthermometry was combined with micro-Raman spectroscopy on doubly polished thick sections (~ 0.15 mm) using a LINKAM THSMG600 heating-freezing stage with an operating range from -196°C up to +600°C (Shepherd et al., 1985), at the University of Graz. Thermally-induced phase transition temperatures, densities and chemical systems of fluid inclusions were observed to determine formation condi-

tions for quartz veins within the blueschists-facies micaschists.

Abbreviations and terminology are referred to Diamond (2003): apparent eutectic temperature  $T_e$  (Antarctite+Hydrohalite+Ice+V  $\rightarrow$  Hydrohalite+Ice+L+V); final melting temperature  $T_m$ (Ice+L+V  $\rightarrow$  L+V), e.g.  $T_m$ (Ice),  $T_m$ (Hydrohalite),  $T_m$ (Halite); total homogenisation temperature  $T_h$ (L+V  $\rightarrow$  L or V).

Fluid inclusion compositions were determined using the three component system H<sub>2</sub>O-NaCl-CaCl<sub>2</sub> based on Steele-MacInnis et al. (2011). In order to identify constituents in wt. % (e.g.  $X_{NaCl}$ ,  $X_{CaCl_2}$ ), final melting temperature of halite was evaluated in the

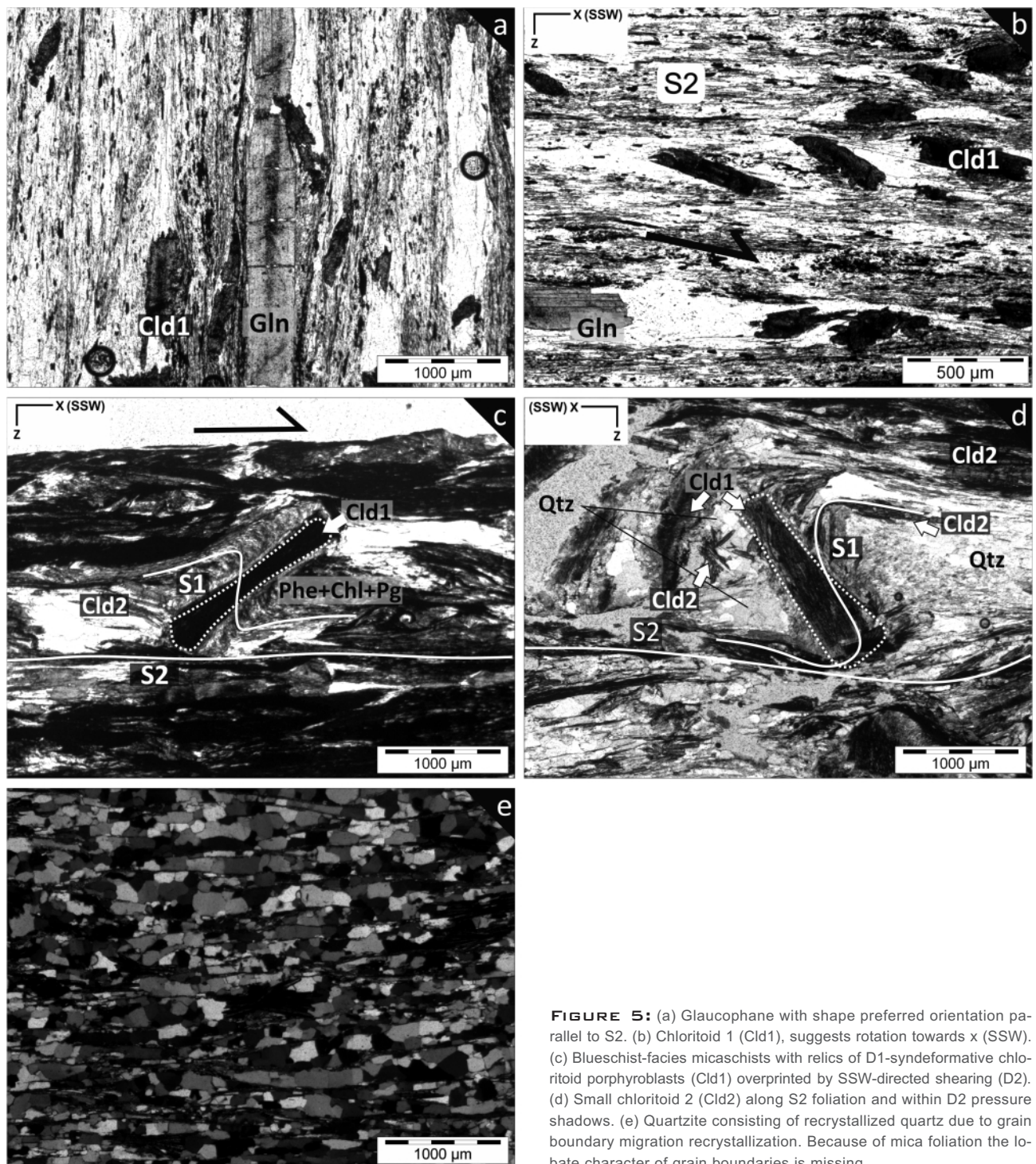


**FIGURE 5:** (a) Glaucophane with shape preferred orientation parallel to S2. (b) Chloritoid 1 (Cld1), suggests rotation towards x (SSW). (c) Blueschist-facies micaschists with relics of D1-syn-deformative chloritoid porphyroblasts (Cld1) overprinted by SSW-directed shearing (D2). (d) Small chloritoid 2 (Cld2) along S2 foliation and within D2 pressure shadows. (e) Quartzite consisting of recrystallized quartz due to grain boundary migration recrystallization. Because of mica foliation the lobate character of grain boundaries is missing.

H<sub>2</sub>O-NaCl-CaCl<sub>2</sub> system. To determine  $X_{\text{NaCl}} \cdot X_{\text{CaCl}_2}$ , observations of Samson and Walker (2000) were used. Densities and amount-of-substance fractions were calculated with the software BULK (Bakker, 2003). For this,  $T_m(\text{Ice})$ ,  $T_n$  and relative NaCl- and CaCl<sub>2</sub>-values with equations according to Naden (1996) and Oakes et al. (1990) in a manually defined system (H<sub>2</sub>O-NaCl-CaCl<sub>2</sub>) were used. Salinity of solid phase halite was calculated after Bodnar (2003). Isochores were estimated with the software ISOC (Bakker, 2003) using the equation of state after Zhang and Frantz (1987).

Low temperature micro-Raman spectroscopy was performed down to -190°C with a HORIBA JOBIN YVON LabRam-HR 800 micro-Raman spectrometer at the University of Graz. A 50 mW Ar<sup>+</sup>-laser with the 532 nm emission line through an OLYMPUS 100X objective (N.A. 0.9) was used. Thus a laser spot with a diameter of about 1 µm and a power of 20 mW was produced on the sample surface. To disperse the light, a holographic grating with 1800 grooves/mm was used. A 1024 x 256 open electrode CCD detector collected the dispersed light. In order to determine the spectral resolution (~ 1.8 cm<sup>-1</sup>), the Rayleigh line of a polished single crystal siliconwafer was measured. To assure an accuracy of Raman band shifts better than 0.5 cm<sup>-1</sup>, the zero-order position of the grating was regularly adjusted and controlled by measuring the Rayleigh line. The detection range for measured crystals of the host rock was 100 - 1600 cm<sup>-1</sup> and for frozen fluid inclusions 2800 to 3700 cm<sup>-1</sup>.

#### 4. FIELD MAPPING AND MACROSTRUCTURES

The mapped area comprises rocks belonging to the Phyllite-Quartzite Unit, such as blueschist-facies micaschists, blueschists, metaconglomerates, and quartzites, and rocks belonging to the Plattenkalk Unit, which are medium-grade marbles and calcareous micaschists with inclusions of elongated marble clasts and boulders. Structural mapping of an area of about 4 km<sup>2</sup> revealed the distinction of three deformation stages. Deformation stage D1 is represented by structures resulting

from uniaxial stretching like tight F1 folds with steep SW-plunging fold axes parallel to the stretching lineation or the apparent preferred orientation of minerals like quartz, zoisite and glaucophane, also aligned parallel to the direction of stretching (see Figs. 3a and b and chapter below). Perpendicular to stretching, F1-folds occur and no clear foliation is visible in these rocks. The occurrence of D1 is restricted to blueschist facies rocks, i.e. glaucophane - chloritoid-rich lenses and layers within quartz-rich metaconglomerates (Fig. 3c). Deformation stage D2 is characterized by SW-directed shearing and the occurrence of asymmetric shear folds F2 with S- to SE-plunging fold axes (Fig. 3d). Deformation stage D3 is characterized by open F3-folds with shallow, W-E trending fold axes (Fig. 3e). Superposition of folding events F2 and F3 forms a km-scale type-2 fold interference pattern (referring to Ramsay and Huber, 1987) (Fig. 4). Concordant quartz layers and discordant quartz-filled veins occur frequently. The latter indicate predominantly N-S directed extension (deformation stage D4). Both vein types were sampled for fluid inclusion analysis as Qtz1 (layer-parallel) and Qtz2 (discordant).

### 5. PETROGRAPHY AND STRUCTURAL ANALYSIS

Blueschists, metaconglomerates and quartzites are embedded as layers and boudins in blueschist-facies micaschists.

#### 5.1 BLUESCHISTS

The dominant deformation event in blueschists shows stretching parallel to the dominant field stretching lineation and no foliation is developed in sections perpendicular to it. This is evident for D1 uniaxial stretching. The mineral assemblage is glaucophane + chloritoid 1 + phengite + quartz. Glaucophane forms elongated grains (up to 2.5 mm in-size) and is together with chloritoid 1 always aligned parallel to S2, and surrounded by phengite and quartz (Figs. 5a and b).

After Leake et al. (1997) and Mogessie et al. (2004) amphiboles can be classified as sodic, with glaucophane as end member (Figs. 6a and b). Na<sub>2</sub>O contents range between 7.68 and

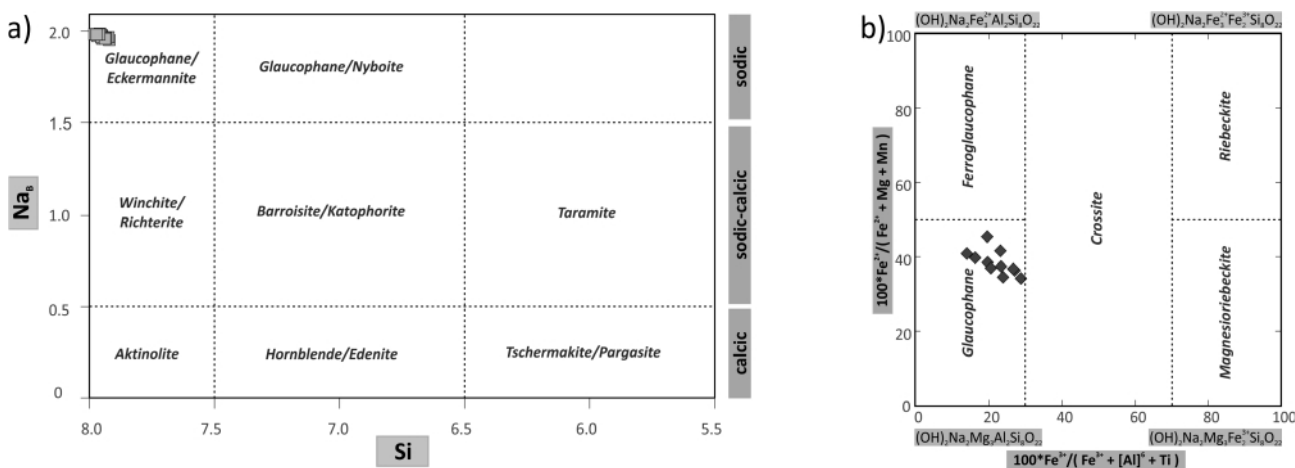


**FIGURE 6:** (a) Amphibole classification after Leake et al. (1997) and Mogessie et al. (2004). Chemistry of studied amphiboles plots in the glaucophane field. (b) Mineral chemistry of sodic amphiboles in a  $100^*Fe^{2+}/(Fe^{2+} + Mg + Mn)$  vs.  $100^*Fe^{2+}/(Fe^{2+} + [Al]^6 + Ti)$  diagram. Chemical compositions indicate glaucophane.

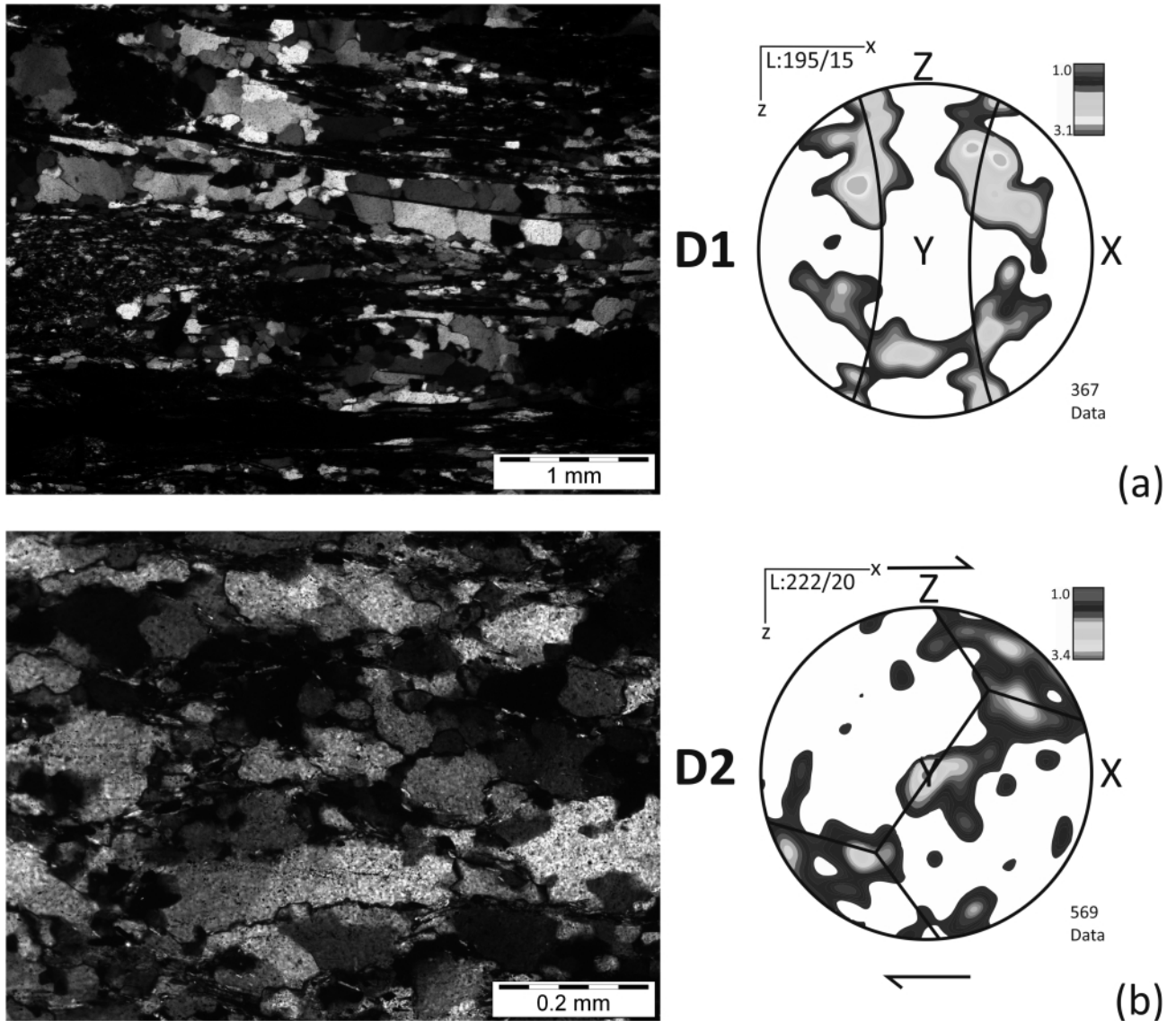


**FIGURE 7:** LPO plots combined with microstructures from the blueschist-facies micaschists (a) and metaconglomerates (b). (a) Left: fine grained quartz (< 0.7 mm) showing grain boundary migration (GBM) recrystallization. Right: quartz c-axes distribution indicates a prolate geometry and is linked with D1. (b) Left: quartz (< 0.6 mm) shows undulatory extinction as well as bulging recrystallization and core-mantle textures. Quartz c-axes distribution displays a cross-girdle pattern of type 1 after Lister (1977). Asymmetry points to SW-directed shearing and is linked with D2.

8.41 wt. %. CaO (0.32 wt. %) and K<sub>2</sub>O (0.12 wt. %) are only present in trace amounts. Compared to FeO values (~ 13.9 wt. %), MgO values (~ 9.5 wt. %) are significantly lower.

Chloritoid 1 exhibits FeO contents between 24.47 and 26.83 wt. %, average MgO of ~ 2.74 wt. %, and insignificant contents of MnO (0.01 - 0.94 wt. %).

Phengites display average K<sub>2</sub>O, FeO and MgO values of ~ 7.72 wt. %, ~ 4.54 wt. % and ~ 3.28 wt. %, respectively.

## 5.2 BLUESCHIST-FACIES MICASCHISTS

Micaschists consist of two generations of chloritoid (Cld1 and Cld2) + phengite + paragonite + chlorite + graphite + quartz. Syndeformative chloritoid porphyroblasts (Cld1) up to 2 mm in size enclose an earlier internal foliation S1 (D1) and are retrogressed to white mica (phengite), chlorite and graphite. This retrogression resulted from the SSW-directed shearing of the Phyllite-Quartzite Unit (D2) linked with the formation of the do-

minant field foliation S2 (Fig. 5c). The internal foliation S1 continues into the external foliation S2 (Figs. 5c and d). Chloritoid 2 (Cld2) reaches a size of up to 0.8 mm and is arranged in clusters or as foliation-parallel grains up to 1.8 mm. Quartz (< 0.7 mm in-size) dominates within the fine grained matrix but is also found as much smaller crystals (< 0.05 mm) within pressure shadows (Fig. 5d). Due to the presence of lobate grain boundaries the matrix quartz shows typical features of grain boundary migration recrystallization (GBM) (Stipp et al., 2002).

Compared to chloritoid compositions in blueschists (Cld1), those in blueschist-facies micaschists (Cld2) display lower FeO values (22.50 - 24.20 wt. %). MgO contents, however, exhibit average amounts of ~2.32 wt. %, similar to chloritoids in the blueschists. Phengites show FeO and MgO values up to 2.3 wt. % and 2.99 wt. %, respectively. Due to exchange reactions with paragonite, their Na<sub>2</sub>O contents can reach up

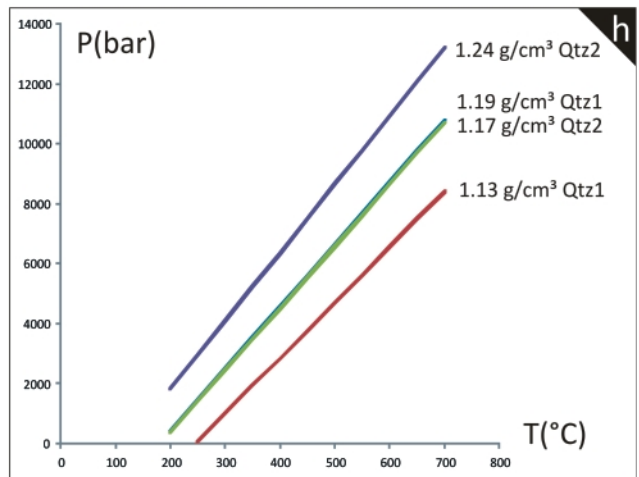
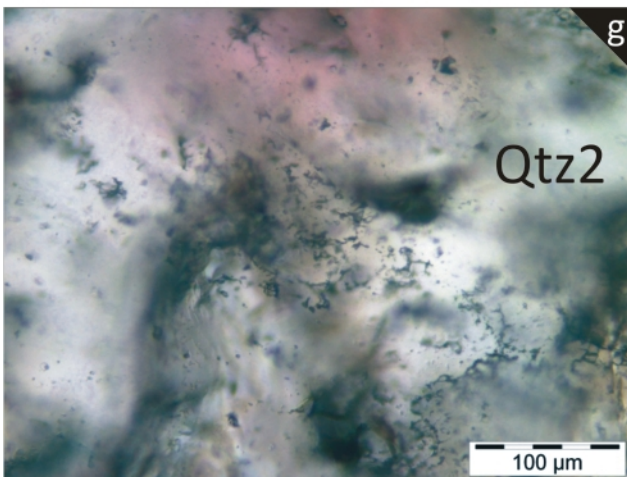
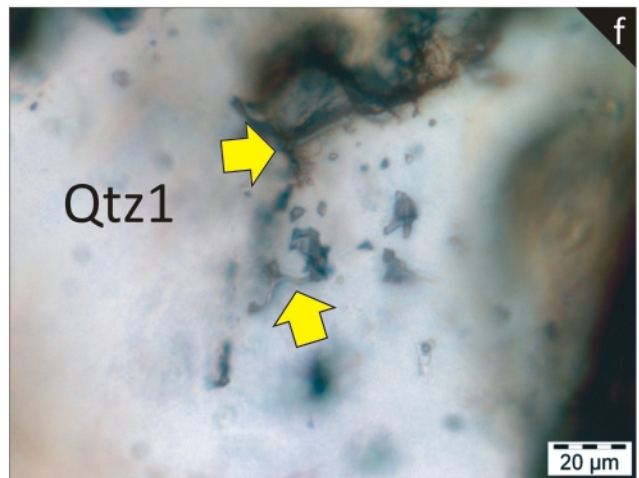
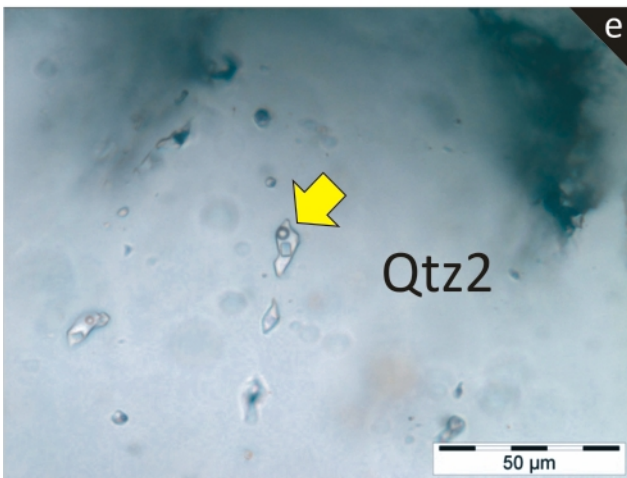
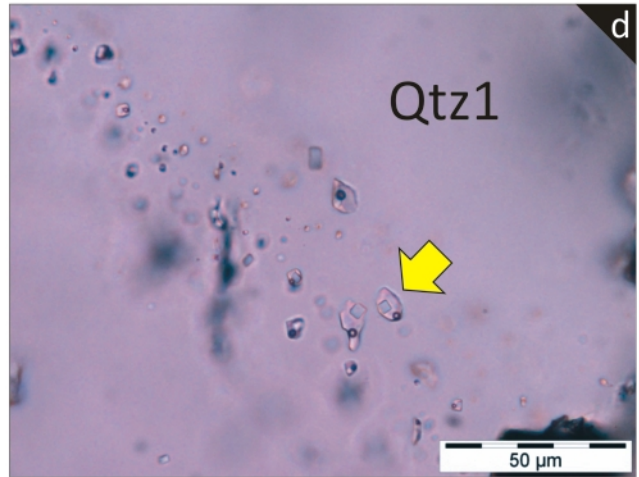
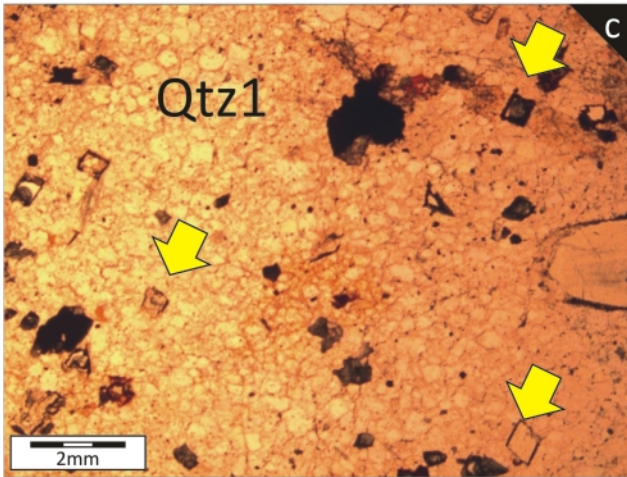
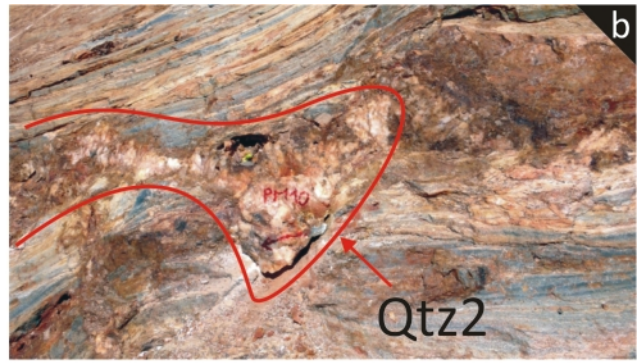


**FIGURE 8:** (a) Concordant quartz vein (Qtz1). (b) Discordant quartz vein (Qtz2). (c) Recrystallized fine-grained quartz matrix (Qtz1) including mm-scale dolomite crystals (yellow arrows). (d) Polyphase (L,V,S) fluid inclusions arranged along intragranular fluid inclusion planes (Qtz1). (e) Polyphase (L,V,S) single fluid inclusions in Qtz2. (f) Hook-like morphology and planes of small inclusions (see arrows) indicative for ITD after Vityk and Bodnar (1995). (g) Irregular dendritic inclusion texture in Qtz2 indicating IBC after Vityk and Bodnar (1995). (h) Calculated isochores from fluid inclusions (densities between 1.19 and 1.13 g/cm<sup>3</sup> for Qtz1 and 1.24 to 1.19 g/cm<sup>3</sup> for Qtz2).

to 2.52 wt. %. The ones aligned parallel to the foliation, however, exhibit higher MgO contents (3.5 - 4.04 wt. %). Their Na<sub>2</sub>O values do not exceed 0.2 wt. %.

Paragonites, when in contact with phengites, display Na<sub>2</sub>O values between 5.37 and 8.14 wt. %, whereas FeO (~0.72 wt. %) and MgO (~0.4 wt. %) are present in trace amounts.

### 5.3 METACONGLOMERATES

Metaconglomerates consist of quartz + feldspar + chloritoid

2 + mica ± glaucophane. Glaucophane and chloritoid are rather rarely preserved.

### 5.4 QUARTZITES

Quartzites consist of quartz + chloritoid 2 + mica + chlorite. Accessories are tourmaline and rutile. Fine grained quartz and chloritoid build up the matrix with grain sizes up to 0.5 mm and 1 mm, respectively. Chloritoid is arranged as clusters and widely distributed, overgrowing the penetrative foliation S<sub>2</sub>; this suggests post-deformative growth with regard to D<sub>2</sub>. Microstructures in quartz show GBM, indicative for minimum temperatures of about 500°C (Stipp et al., 2002) (Fig. 5e).

### 6. LATTICE PREFERRED ORIENTATION OF QUARTZ

Sections have been cut parallel to the dominant field stretching lineation which results from D<sub>1</sub> uniaxial stretching (L<sub>1</sub>) and the subsequent re-orientation during D<sub>2</sub> non-coaxial shearing (L<sub>2</sub>). Blueschist-facies micaschists show a symmetric small circle distribution of quartz c-axes on both sides of the y-z plane

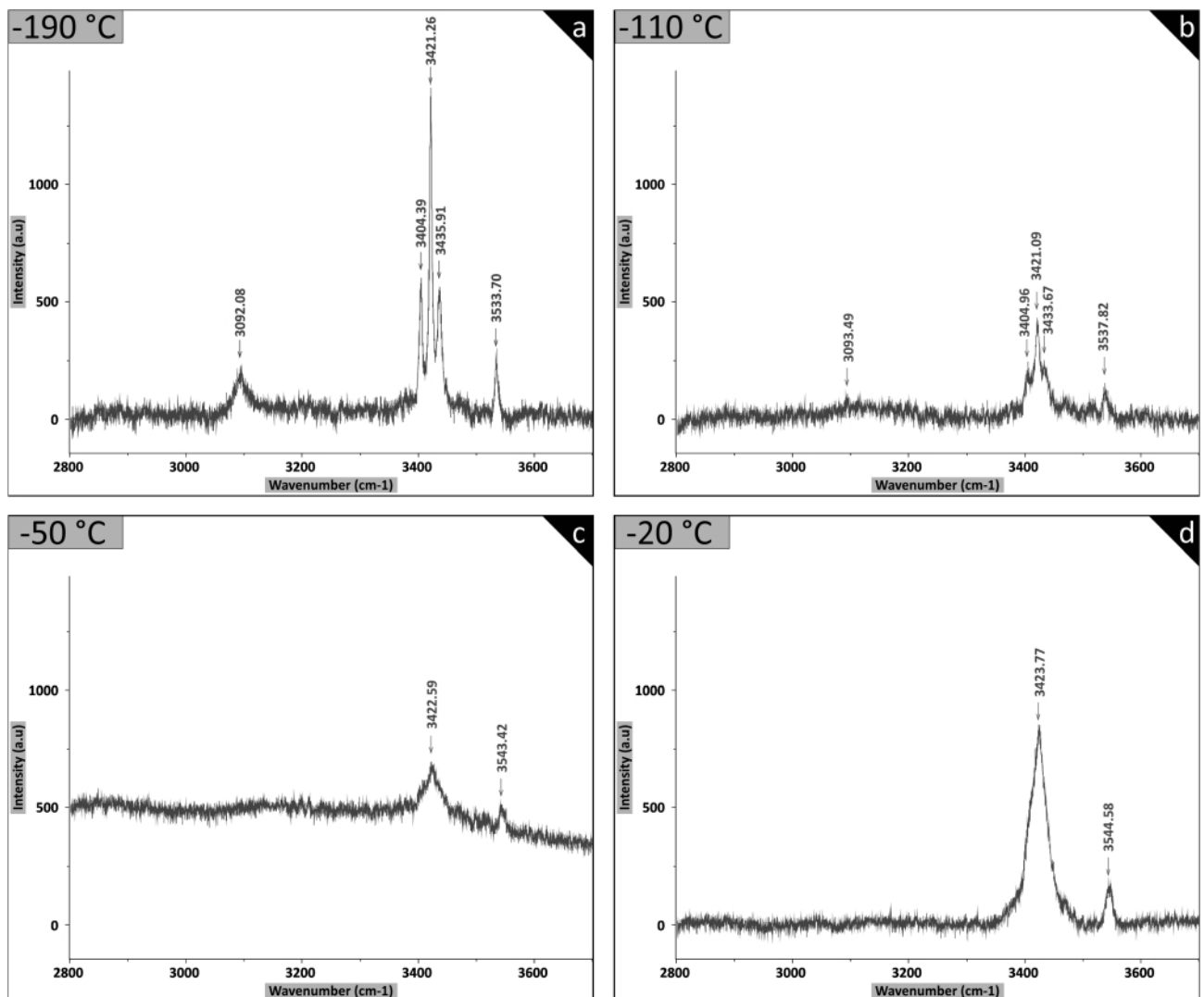


**FIGURE 9:** (a)-(d) Low-temperature Raman spectra of fluid inclusions from -190°C to -20°C. Spectra show ice peak at ca. 3093 cm<sup>-1</sup> and dominant peaks of a mixture of hydrohalite and antarctite at higher wavenumbers. Note that ice peak disappears at temperatures > -110°C. Dominant peaks at temperatures > -50°C are attributed to hydrohalite.

that is typical for uniaxial stretching (Fig. 7a) (Passchier and Trouw, 2005). Quartz grains (< 0.7 mm in-size) within the fine grained layers exhibit GBM recrystallization. Fine-grained layers of metaconglomerate show quartz grains (< 0.6 mm in-size) which exhibit undulatory extinction and bulging, as well as core and mantle textures (Fig. 7b). Lattice preferred orientation is characterized by dominant maxima at  $\gamma$ , which points to prism  $\langle a \rangle$  gliding. Further active glide systems are assumed to be rhomb  $\langle a \rangle$  and basal  $\langle a \rangle$  gliding. A cross-girdle distribution pattern of type 1 (Lister, 1977) indicates shearing towards SW, during D2.

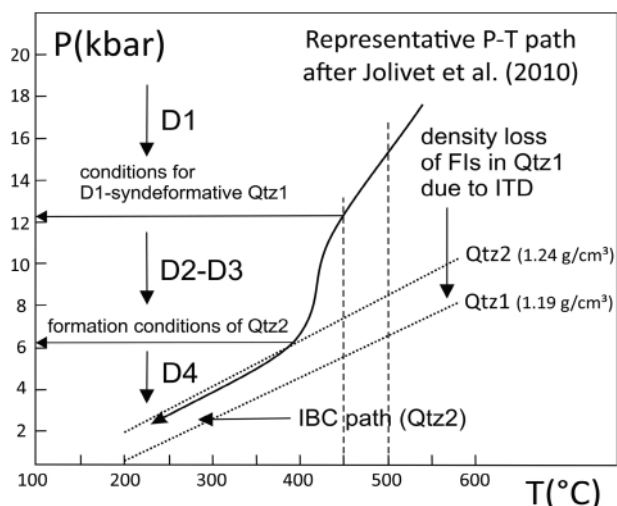


**FIGURE 10:** Representative P-T path for blueschists of the southern Peloponnese crossed with calculated isochores from fluid inclusions in Qtz1 and Qtz2. Conditions for Qtz2 constrain deformation stages D1-D3 above 6 kbar and <400°C. Lower P-T conditions from fluid inclusions of Qtz1 are interpreted as density-loss due to fluid inclusion re-equilibration.

## 7. FLUID INCLUSION STUDY

Fluid inclusion microthermometry was performed on doubly polished thick sections of representative samples from a D2 foliation-parallel quartz vein (Qtz1) and a D4-related discordant quartz vein (Qtz2) (Figs. 8a and b). No suitable fluid inclusions were found in the surrounding host rocks (blueschists and blueschist-facies micaschists). Qtz1 consist mainly of recrystallized fine-grained quartz grains ( $\leq 0.8$  mm) which occur together with euhedral dolomite crystals ( $\leq 1.2$  mm). Dolomite was identified by Raman spectroscopy (e.g. Baumgartner and Bakker, 2010). No dolomite crystals have been found as solid phase in fluid inclusions. Qtz2 consists of coarse grained quartz (> 3 mm) and does not contain dolomite. Qtz1 in general displays fluid inclusions along fluid inclusion planes (Fig. 8d). Qtz2 exhibits fluid inclusions arranged mainly as single clusters (Fig. 8e) or along intragranular fluid inclusion planes.

In general, fluid inclusions display a homogeneous saline fluid both in Qtz1 and Qtz2. On the basis of eutectic temperatures  $T_e$ , microthermometry indicates a  $\text{H}_2\text{O}-\text{NaCl}-\text{CaCl}_2$  chemical system, with halite daughter crystals as solid phase (Figs. 8d and e). After cooling down to  $-190^\circ\text{C}$ , heat runs yield a first change in the relief of fluid inclusions in Qtz1 from darkening to granular at temperatures between  $-73$  and  $-71^\circ\text{C}$ , which is seen as a metastable behavior of antarcticite during melting (e.g. Samson and Walker, 2000). In Qtz2 fluid inclusions show this relief change between  $-75$  to  $-73^\circ\text{C}$ . Final melting of ice  $T_m(\text{Ice})$  in Qtz1 and Qtz2 occurred before final melting of hydrohalite and was observed at temperatures from  $-50$  to  $-47^\circ\text{C}$  and  $-51$  to  $-49^\circ\text{C}$ , respectively. The final melting of a solid phase assumed to be hydrohalite occurred around  $-35^\circ\text{C}$ . The ranges in homogenization temperatures  $T_h$  of fluid inclusions in Qtz1 (180 to  $248^\circ\text{C}$ ) and Qtz2 (120 to  $182^\circ\text{C}$ ) result in different densities from 1.19 to  $1.13\text{ g/cm}^3$  and 1.24 to  $1.17\text{ g/cm}^3$ , respectively. Melting of halite occurred between 290 and  $390^\circ\text{C}$  in Qtz1 and between 270 and  $387^\circ\text{C}$  in Qtz2 indicating almost the same salinities between 36 and 46 wt. % after Bodnar (2003). Evidence for a non-isochoric P-T evolution of the host rocks of Qtz1 and Qtz2 is given by decrepitation textures which indicate isothermal decompression (ITD) in Qtz1 and isobaric cooling (IBC) in Qtz2 after Vityk and Bodnar (1995) (Figs. 8f and g). Respective isochores for both types of quartz veins are given in Fig. 8h.

Low temperature Raman spectroscopy of fluid inclusions from Qtz1 shows peaks typical for a mixture of hydrohalite and antarcticite in the range between  $-190$  to  $-50^\circ\text{C}$  and a significant broad peak for hydrohalite up to temperatures near  $0^\circ\text{C}$ . This points to a metastable behavior of hydrohalite in

Qtz	Deformation style	n	Textural appearance	Size (mm)	n*/phases	$T_e$ ( $^\circ\text{C}$ )	$T_m(\text{Ice})$ ( $^\circ\text{C}$ )	$T_m(\text{Hydrohalite})$ ( $^\circ\text{C}$ )	$T_h(\text{partial})$ ( $^\circ\text{C}$ )	$T_m(\text{Halite})$ ( $^\circ\text{C}$ )	Total salinity	Density ( $\text{g/cm}^3$ )	Chemistry
													H <sub>2</sub> O - NaCl - CaCl <sub>2</sub>
1	concordant	15	intragranular FIP	< 0.8	3/L-V-S	< -52	-50 to -47	-37 to -34	182 to 248	290 to 390	37.4 to 46.4	1.13 to 1.19	H <sub>2</sub> O - NaCl - CaCl <sub>2</sub>
2	discordant	20	intragr. FIP cluster, single	> 3	3/L-V-S	< -52	-51 to -49	-35	120 to 182	270 to 387	36 to 46.4	1.17 to 1.24	H <sub>2</sub> O - NaCl - CaCl <sub>2</sub>

**TABLE 1:** Microthermometric data of studied fluid inclusions. Abbreviations: n...number of fluid inclusions; n\*... number of phases at room temperatures;  $T_e$ ...eutectic temperature;  $T_m(\text{Ice})$ ...last melting temperature of ice;  $T_m(\text{Hydrohalite})$ ...last melting temperature of hydrohalite;  $T_m(\text{Halite})$ ...last melting temperature of halite;  $T_h(\text{partial})$ ... total homogenization to the liquid phase by the presence of halite.

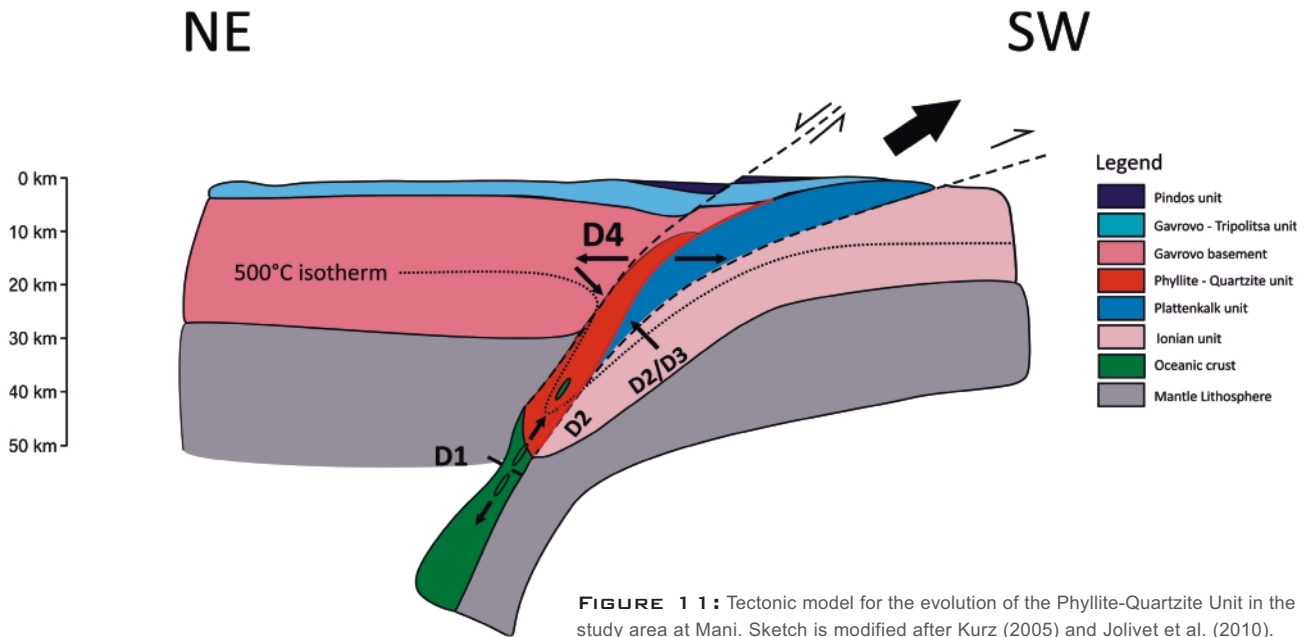


**FIGURE 11:** Tectonic model for the evolution of the Phyllite-Quartzite Unit in the study area at Mani. Sketch is modified after Kurz (2005) and Jolivet et al. (2010).

most fluid inclusions (Fig. 9). A similar intensity of the 3404 and 3436  $\text{cm}^{-1}$  peaks is indicative for a fluid composition of  $X_{\text{NaCl}}/X_{\text{CaCl}_2} = 2:1$  (after Samson and Walker, 2000). At temperatures up to  $-20^\circ\text{C}$  the dominant peaks at 3423.77  $\text{cm}^{-1}$  and 3544.58  $\text{cm}^{-1}$  can be clearly attributed to hydrohalite.

## B. SUMMARY AND INTERPRETATION

The Phyllite-Quartzite Unit was affected by uniaxial stretching during the earliest observable deformation stage (F1-constriction folds) at high-pressure conditions, documented by the syndeformative growth of glaucophane and Cld1. In blueschist-facies micaschists Cld1 porphyroblasts with an internal foliation S1 belong to D1 and appear as texturally equal to syndeformative D1 porphyroblasts described by Xypolias et al. (2007). D2 is contemporaneous to retrogression of Cld1 into phengite and chlorite and to the formation of Cld2. The latter is always aligned to the S2 foliation and S2 pressure shadows. In blueschists, Cld1 and Gln appear as syngenetic and were rotated towards the S2 foliation. Observed deformation stages are linked with age data proposed by Chatzaras et al. (2013) and references therein (see chapter Geological Setting). D1 can be related to a time range between 29 and 24 Ma and D2 in the range between 24 and 19 Ma. This would also include D3 at a late stage around 19 Ma. D4 extension is linked with a time range between 19 and 15 Ma.

Assuming peak pressure conditions of about 13-17 kbar after Xypolias et al. (2007) in combination with a representative P-T path after Jolivet et al. (2010) for the southern Peloponnese (Fig. 10), the Phyllite-Quartzite Unit which was subducted to depths of about 40 to 50 km. Subsequent exhumation was accompanied by D1 uniaxial stretching and the growth of former mentioned syndeformative minerals like glaucophane and Cld1. The occurrence of Qtz1 as concordant quartz vein, which deformed due to grain boundary migration recrystallization at ca. 450-500°C, suggests formation of Qtz1 near peak

metamorphic conditions before deformation stage D2. Estimated isochores from fluid inclusion study do not indicate peak metamorphic conditions. By crossing temperature isotherms with calculated isochores from Qtz1, maximum pressure conditions between 6 and 7 kbar at 500°C can be estimated (Fig. 10). These lower pressures are the result of density loss due to non-isochoric exhumation after fluid entrapment. This is supported by decrepitation textures in Qtz1 (Fig. 10). Higher densities were calculated from fluid inclusions in discordant Qtz2 that support density loss of fluid inclusions in Qtz1 due to recrystallization and subsequent density re-equilibration of earlier large fluid inclusions. Formation conditions of Qtz1 can therefore be more likely linked with early exhumation stages during the proposed P-T evolution after Jolivet et al. (2010) which would indicate pressures between 13 and 16 kbar. This would suggest density loss of up to 10 kbar as result of ITD in Qtz1. Concerning the fact that Qtz2 is clearly discordant to the surrounding blueschist-facies micaschists, which also experienced D1-D3, the assumed conditions for Qtz2 near 6 kbar and  $<400^\circ\text{C}$  constrain minimum pressures and temperatures for D1-D3 in the Phyllite-Quartzite Unit.

The structural evolution at the pressure peak and along the earliest exhumation path is dominated by constriction (Fig. 11). Therefore, it is proposed that crustal lithosphere was subducted due to slab pull which requires a more dense oceanic crust followed by slab break-off and D1 uniaxial stretch (e.g. Kurz, 2005). D1 continues into SSW to SW-directed shear (deformation stage D2) forming a NE-dipping tectonic wedge. Subsequent late-stage open folding (D3) resulted into large-scale F2/F3 fold interference. Minimum P-T conditions for D1-D3 are constrained by the formation of D4 related veins which indicate subsequent extension in the region at Mani peninsula.

## ACKNOWLEDGEMENTS

This work results from a field mapping course and a one year

later sample excursion. The authors are therefore highly appreciated to all the participants of this lecture in the year 2007. In addition, P. Xypolias and his PhD student are gratefully acknowledged for their field support and intense discussions in 2007.

Additionally we thank Hans-Jürgen Gawlick and two reviewers A. Kiliias and N. Froitzheim for their fruitful critics and suggestions.

## REFERENCES

- Bakker, R.J., 2003. Package Fluids 1 Computer programs for analysis of fluid inclusion data and for modelling bulk fluid properties. *Chemical Geology*, 194, 3-23. [http://dx.doi.org/10.1016/S0009-2541\(02\)00268-1](http://dx.doi.org/10.1016/S0009-2541(02)00268-1)
- Baumgartner, M. and Bakker, R. J., 2010). Raman spectra of ice and salt hydrates in synthetic fluid inclusions. *Chemical Geology*, 275, 58-66. <http://dx.doi.org/10.1016/j.chemgeo.2010.04.014>
- Bizon, G., Bonneau, M., Leboulenger, P., Matesco, S. and Thiebault, F., 1976. Sur la signification et l'extension des "massifs cristallins externes" en Péloponnèse méridional et dans l'Arc égéen. *Bulletin de la Société géologique de France*, 18, 337-345.
- Blumör, T., Dollinger, J., Knobel, M., Mutter, A., Zarda, S. and Kowalczyk, G., 1994. Plattenkalk series and Kastania Phyllites of the Taygetos Mts, new results on structure and succession. *Bulletin of the Geological Society of Greece*, 30 (2), 83-92.
- Bodnar, R.J., 2003. Introduction to aqueous-electrolyte fluid inclusions. In: I. Samson, A. Anderson and D. Marshall (eds.), *Fluid Inclusions: Analysis and Interpretation*. Mineralogical Association of Canada Short Course Series, 32, pp. 81-99.
- Bonneau, M., 1973. Sur les affinités ioniennes des «calcaires en plaquettes» épimétamorphiques de la Crète, le charriage de la série de Gavrovo-Tripolitsa et la structure de l'arc égéen. *Comptes Rendus de l'Académie des Sciences*, 277, 2453-2456.
- Boullier, A.M., Lanord, C.F., Dubessy, J., Adamy, J. and Champenois, M., 1991. Linked fluid and tectonic evolution in the High Himalayan mountains (Nepal). *Contributions to Mineralogy and Petrology*, 107, 358-372.
- Boullier, A.M., 1999. Fluid inclusions: tectonic indicators. *Journal of Structural Geology*, 21, 1229-1235.
- Chatzaras, V., Xypolias, P. and Doutsos, T., 2006. Exhumation of high-pressure rocks under continuous compression: a working hypothesis for the southern Hellenides (central Crete, Greece). *Geological Magazine*, 143, 859-876. <http://dx.doi.org/10.1017/S0016756806002585>
- Chatzaras, V., Xypolias, P., Kokkalas, S. and Koukouvelas, I., 2013. Tectonic evolution of a crustal-scale oblique ramp, Hellenides thrust belt, Greece. *Journal of Structural Geology*, 57, 16-37. <http://dx.doi.org/10.1016/j.jsg.2013.10.003>
- Diamond, L., 2003. Glossary: Terms and symbols used in fluid inclusion studies. In: I. Samson, A. Anderson and D. Marshall (eds.), *Fluid Inclusions: Analysis and Interpretation*. Mineralogical Association of Canada Short Course Series, 32, pp. 365-374.
- Doutsos, T., Koukouvelas, I., Poulimenos, G., Kokkalas, S., Xypolias, P. and Skourlis, K., 2000. An exhumation model of the south Peloponnesus, Greece. *International Journal of Earth Sciences*, 89, 350-365.
- Doutsos, T., Koukouvelas, I. and Xypolias, P., 2006. A new orogenic model for the External Hellenides. In: A.H.F. Robertson and D. Mountrakis (eds), *Tectonic evolution of the Eastern Mediterranean regions*. Geological Society London Special Publications, 260, pp. 507-520.
- Fassoulas, C., Kiliias, A. and Mountrakis, D., 1994. Post-nappe stacking extension and exhumation of the HP-LT rocks in the island of Crete, Greece. *Tectonics*, 13, 127-138.
- Jacobshagen, V., 1986. *Geologie von Griechenland*. Beiträge zur regionalen Geologie der Erde. Gebrüder Borntraeger, Berlin-Stuttgart, 363 pp.
- Jolivet, L., Daniel, J.M., Truffert, C. and Goffé, B., 1994b. Exhumation of deep crustal metamorphic rocks and crustal extension in back-arc regions. *Lithos*, 33(1/2), 3-30.
- Jolivet, L. and Faccenna, C., 2000. Mediterranean extension and the Africa-Eurasia collision. *Tectonics*, 19, 1095-1106. <http://dx.doi.org/10.1029/2000TC900018>
- Jolivet, L., Faccenna, C., Goffé, B., Burov, E., and Agard, P., 2003. Subduction tectonics and exhumation of high-pressure metamorphic rocks in the Mediterranean orogens. *American Journal of Science*, 303, 353-409. <http://dx.doi.org/10.2475/ajs.303.5.353>
- Jolivet, L., Trotet, F., Monié, P., Vidal, O., Goffé, B., Labrousse, L., Agard, P. and Ghorbal B., 2010. Along-strike variations of P-T conditions in accretionary wedges and syn-orogenic extension, the HP-LT Phyllite-Quartzite Nappe in Crete and the Peloponnese. *Tectonophysics*, 480, 133-148. <http://dx.doi.org/10.1016/j.tecto.2009.10.002>
- Katagas, C., 1980. Ferroglaucophane and chloritoid-bearing metapelites from the phyllite series, southern Peloponnese, Greece. *Mineralogical Magazine*, 43, 975-978.
- Kiliias, A., Fassoulas, C. and Mountrakis, D., 1994. Tertiary extension of continental crust and uplift of Psiloritis metamorphic core complex in the central part of the Hellenic arc (Crete, Greece). *Geologische Rundschau*, 83, 417-430.

- Krahl, J., Richter, D., Forster, O., Kozur, H. and Hall, R., 1988. Zur Stellung der Talea Ori Deckenstapels (Griecheland). *Zeitschrift der deutschen geologischen Gesellschaft*, 139, 191-227.
- Krenn, K., 2010. Fluid inclusions in quartz related to subsequent stages of foliation development during a single metamorphic cycle (Schneeberg Fault Zone, Eastern Alps, Austria). *Lithos*, 118, 255-268. <http://dx.doi.org/10.1016/j.lithos.2010.05.004>
- Krenn, K., Bauer, C., Proyer, A., Mposkos, E. and Hoinkes, G., 2008. Fluid entrapment and reequilibration during subduction and exhumation: A case study from the high-grade Nestos shear zone, Central Rhodope, Greece. *Lithos*, 104, 33-53. <http://dx.doi.org/10.1016/j.lithos.2007.11.005>
- Kurz, W., 2005. Constriction during exhumation: Evidence from eclogite microstructures. *Geology*, 33, 37-40. <http://dx.doi.org/10.1130/G20887.1>
- Leake, B.E., Woolley, A.R., Arps, C.E.S., Birch, W.D., Gilbert, M.C., Grice, J.D., Hawthorne, F.C., Kato, A., Kisch, H.J., Krivovichev, V.G., Linthout, K., Laird, J., Mandarino, J.A., Maresch, W.V., Nickel, E.H., Rock, N.M.S., Schumacher, J.C., Smith, D. C., Stephenson, N.C.N., Ungaretti, L., Whittaker, E.J.W. and Youzhi, G., 1997. Nomenclature of Amphiboles: Report of the subcommittee on amphiboles of the international mineralogical association, commission on new minerals and mineral names. *The Canadian Mineralogist*, 35, 219-246.
- Lespinasse, M. and Pechêr, A., 1986. Microfractures and regional stress field: a study of the preferred orientations of fluid inclusion planes in a granite from the Massiv Central, France. *Journal of Structural Geology*, 8, 169-180.
- Lister, G., 1977. Discussion: crossed-girdle c-axis fabrics in quartzites deformed by plane strain and progressive simple shear. *Tectonophysics*, 39, 51-54.
- Mogessie, A., Ettinger, K. and Leake, B.E., 2004. Nomenclature of amphiboles: Additions and revisions to the International Mineralogical Association's amphibole nomenclature. *Mineralogical Magazine*, 68, 209-215. <http://dx.doi.org/10.1180/0026461046810182>
- Naden, J., 1996. CalcicBrine: a Microsoft Excel 5.0 Add-in for calculating salinities from microthermometric data in the system NaCl-CaCl<sub>2</sub>-H<sub>2</sub>O. PACROFI VI abstract, Wisconsin, USA, pp. 97-98.
- Oakes, C.S., Bodnar, R.J. and Simonson, T.M., 1990. The system NaCl-CaCl<sub>2</sub>-H<sub>2</sub>O: The ice liquidus at 1 atm total pressure. *Geochimica et Cosmochimica Acta*, 54, 603-610.
- Passchier, C.W. and Trouw, R., 2005. *Microtectonics*. Springer-Verlag, Berlin Heidelberg, 366 pp.
- Ramsay, J.G. and Huber M.I., 1987. *The techniques of modern structural geology: Volume 2: Folds and fractures*. Academic Press, London, 800 pp.
- Ring, U., Layer, P.W. and Reischmann, T., 2001. Miocene high-pressure metamorphism in the Cyclades and Crete, Aegean Sea, Greece: Evidence for large-magnitude displacement on the Cretan detachment. *Geology*, 29, 395-398.
- Ring, U. and Reischmann, T., 2002. The weak and superfast Cretan detachment, Greece: Exhumation at subduction rates in extruding wedges. *Journal of the Geological Society London*, 159, 225-228.
- Ring, U., Will, T., Glodny, J., Kumerics, C., Gessner, K., Thomson, S., GÜNGÖR, T., Monié, P., Okrusch, M., and Drüppel, K., 2007. Early exhumation of high-pressure rocks in extrusion wedges: Cycladic blueschists in the eastern Aegean, Greece, and Turkey. *Tectonics*, 26, 1-23. <http://dx.doi.org/10.1029/2005TC001872>
- Robertson, A., 2002. Overview of the genesis and emplacement of Mesozoic ophiolites in the Eastern Mediterranean Tethyan region. *Lithos*, 65(1-2), 1-67. [http://dx.doi.org/10.1016/S0024-4937\(02\)00160-3](http://dx.doi.org/10.1016/S0024-4937(02)00160-3)
- Robertson, A., 2006. Sedimentary evidence from the south Mediterranean region (Sicily, Crete, Peloponnese, Evia) used to test alternative models for the regional tectonic setting of Tethys during Late Palaeozoic-Early Mesozoic time. In: A.H.F. Robertson, and D. Mountrakis (eds.), *Tectonic Development of the Eastern Mediterranean region*. Geological Society London Special Publications, 260, pp. 91-154.
- Samson, I.M. and Walker, R.T., 2000. Cryogenic Raman spectroscopic studies in the system NaCl-CaCl<sub>2</sub>-H<sub>2</sub>O and implications for low temperature phase behaviour in aqueous fluid inclusions. *The Canadian Mineralogist*, 38(1), 35-43.
- Schmid, S.M., Bernoulli, D., Fügenschuh, B., Matenco, L., Schefer, S., Schuster, R., Tischler, M. and Ustaszewski K., 2008. The Alpine-Carpathian-Dinaridic orogenic system: correlation and evolution of tectonic units. *Swiss Journal of Geoscience*, 101, 139-183. <http://dx.doi.org/10.1007/s00015-008-1247-3>
- Seidel, E., Kreuzer, H. and Harre, W., 1982. A Late Oligocene/Early Miocene high pressure belt in the External Hellenides. *Geologisches Jahrbuch*, E23, 165-206.
- Shepherd, T., Rankin, A. and Alderton, D., 1985. *A Practical Guide to Fluid Inclusion*. Blackie, London, 239 pp.
- Smith, A., Woodcock, N. and Naylor, M., 1979. The structural evolution of a Mesozoic continental margin, Othris Mountains, Greece. *Journal of the Geological Society*, 136, 589-601.

Stampfli, G. and Borel, G., 2004. The TRANSMED transects in space and time: Constraints on the palaeotectonic evolution of the Mediterranean domain. In: W. Cavazza, F. Roure, W. Spakman, G. Stampfli and P. Ziegler (eds.), *The TRANSMED Atlas - The Mediterranean region from crust to mantle*. Springer, Berlin-Heidelberg, pp. 53-80.

Steele-MacInnis, M., Bodnar, R. and Naden, J., 2011. Numerical model to determine the composition of H<sub>2</sub>O–NaCl–CaCl<sub>2</sub> fluid inclusions based on microthermometric and microanalytical data. *Geochimica et Cosmochimica Acta*, 75, 21-40. <http://dx.doi.org/10.1016/j.gca.2010.10.002>

Stipp, M., Stünitz, H., Heilbronner, R. and Schmid, S., 2002. The eastern Tonale fault zone: a 'natural laboratory' for crystal plastic deformation of quartz over a temperature range from 250 to 700 °C. *Journal of Structural Geology*, 24, 1861-1884. [http://dx.doi.org/10.1016/S0191-8141\(02\)00035-4](http://dx.doi.org/10.1016/S0191-8141(02)00035-4)

Trotet, F., Goffé, B., Vidal, O. and Jolivet, L., 2006. Evidence of retrograde Mg-carpholite in the Phyllite - Quartzite nappe of Peloponnese from thermobarometric modelisation - geodynamic implications. *Geodinamica Acta*, 19, 323-343. <http://dx.doi.org/10.3166/ga.19.323-343>

Vityk, M.O. and Bodnar, R.J., 1995. Do fluid inclusions in high grade metamorphic terranes preserve peak metamorphic density during retrograde decompression? *American Mineralogist*, 80, 641-644.

Xypolias, P. and Koukouvelas, I., 2001. Kinematic vorticity and strain rate patterns associated with ductile extrusion in the Chelmos Shear zone (External Hellenides, Greece). *Tectonophysics*, 338, 59-77. [http://dx.doi.org/10.1016/S0040-1951\(01\)00125-1](http://dx.doi.org/10.1016/S0040-1951(01)00125-1)

Xypolias, P., Chatzaras, V. and Koukouvelas, I., 2007. Strain gradients in zones of ductile thrusting: Insights from the External Hellenides. *Journal of Structural Geology*, 29, 1522-1537. <http://dx.doi.org/10.1016/j.jsg.2007.05.006>

Zhang, Y.G. and Frantz, J.D., 1987. Determination of homogenization temperatures and densities of supercritical fluids in the system NaCl-KCl-CaCl<sub>2</sub>-H<sub>2</sub>O using synthetic fluid inclusions. *Chemical Geology*, 64, 35-350.

Received: 1 April 2014

Accepted: 1 October 2014

Peter MICHEUZ, Kurt KRENN<sup>1</sup>, Harald FRITZ & Walter KURZ  
Institute of Earth Sciences, Member of NAWI Graz, University of Graz,  
Universitätsplatz 2, A-8010 Graz, Austria;

<sup>1</sup> Corresponding author, [kurt.krenn@uni-graz.at](mailto:kurt.krenn@uni-graz.at)